PKU-TP-98-55

Diffractive gluon jet production at hadron colliders in the two-gluon exchange model

Feng Yuan
Department of Physics, Peking University, Beijing 100871, People's Republic of China

Kuang-Ta Chao
China Center of Advanced Science and Technology (World Laboratory), Beijing 100080, People's Republic of China
and Department of Physics, Peking University, Beijing 100871, People's Republic of China

Abstract

Following our recent paper on the calculations of diffractive quark jet production at hadron colliders, we present here the calculations of gluon jet production at hadron colliders in the two-gluon exchange parameterization of the Pomeron model. We use the helicity amplitude method to calculate the cross section formula. We find that for the gluon jet production the diffractive process is related to the differential off-diagonal gluon distribution function in the proton. We estimate the production rate for this process at the Fermilab Tevatron by approximating the off-diagonal gluon distribution function by the usual diagonal gluon distribution.

PACS number(s): 12.40.Nn, 13.85.Ni, 14.40.Gx

I. INTRODUCTION

In recent years, there has been a renaissance of interest in diffractive scattering. These diffractive processes are described by the Regge theory in terms of the Pomeron ($I\!P$) exchange [1]. The Pomeron carries quantum numbers of the vacuum, so it is a colorless entity in QCD language, which may lead to the "rapidity gap" events in experiments. However, the nature of Pomeron and its reaction with hadrons remain a mystery. For a long time it had been understood that the dynamics of the "soft pomeron" is deeply tied to confinement. However, it has been realized now that how much can be learned about QCD from the wide variety of small-x and hard diffractive processes, which are now under study experimentally. In Refs. [2,3], the diffractive J/ψ and Υ production cross section have been formulated in photoproduction processes and in DIS processes in perturbative QCD. In the framework of perturbative QCD the Pomeron is represented by a pair of gluon in the color-singlet sate. This two-gluon exchange model can successfully describe the experimental results from HERA [5].

On the other hand, as we know that there exist nonfactorization effects in the hard diffractive processes at hadron colliders [6–9]. First, there is the so-called spectator effect [8], which can change the probability of the diffractive hadron emerging from collisions intact. Practically, a suppression factor (or survive factor) "S_F" is used to describe this effect [10]. Obviously, this suppression factor can not be calculated in perturbative QCD, which is now viewed as a nonperturbative parameter. Typically, the suppression factor S_F is determined to be about 0.1 at the energy scale of the Fermilab Tevatron [9]. Another nonfactorization effect discussed in literature is associated with the coherent diffractive processes at hadron colliders [7], in which the whole Pomeron is induced in the hard scattering. It is proved in [7] that the existence of the leading twist coherent diffractive processes is associated with a breakdown of the QCD factorization theorem.

Based on the success of the two-gluon exchange parametrization of the Pomeron model in the description of the diffractive photoproduction processes at ep colliders [2,3,5], we may extend the applications of this model to calculate the diffractive processes at hadron colliders in perturbative QCD. Under this context, the Pomeron represented by a color-singlet two-gluon system emits from one hadron and interacts with another hadron in hard process, in which the two gluons are both involved (as shown in Fig. 1). Therefore, these processes calculated in the two-gluon exchange model are just belong to the coherent diffractive processes in hadron collisions. Another important feature of the calculations of the diffractive processes in this model recently demonstrated is the sensitivity to the off-diagonal parton distribution function in the proton [11].

Using this two-gluon exchange model, we have calculated the diffractive J/ψ production [12], quark jet production [13,14], massive muon pair and W boson productions [15], and direct photon production [16] in hadron collisions. In this paper, we will further calculate the gluon jet production at large transverse momentum in the coherent diffractive processes at hadron colliders by using the two-gluon exchange model. In the calculations of Refs. [12,13,15], there always is a large mass scale associated with the production process. That is M_ψ for J/ψ production, m_c for the charm jet production, M^2 for the massive muon production (M^2 is the invariant mass of the muon pair) and M_W^2 for W boson production. However, in the gluon jet production process as well as the light quark jet production process,

there is no large mass scale. So, for these processes, the large transverse momentum is needed to guarantee the application of the perturbative QCD. Furthermore, in [14] we show that the light quark jet production in the two-gluon exchange model has a distinctive feature that there is no contribution from the small l_T^2 region ($l_T^2 < k_T^2$) in the integration of the amplitude over l_T^2. (The similar behavior has also been found for the diffractive light quark photoproduction process [17].) So, the expansion (in terms of l_T^2/M_X^2) method used in Refs. [12,13,15] can not be applied to the calculations of gluon jet production. In the following calculations, we will employ the helicity amplitude method to calculate the amplitude of the diffractive gluon jet production in hadron collisions. We will show that the production cross section is related to the differential (off-diagonal) gluon distribution function in the proton as that in the diffractive light quark jet production process [14]. (On the other hand, we note that the cross sections of the processes calculated in Refs. [12,13,15] are related to the integrated gluon distribution function in the proton).

Diffractive gluon jet production can come from two types partonic processes: one is the quark initiated process (Fig.2), and the other is the gluon initiated process (Fig.3).

The diffractive production of heavy quark jet at hadron colliders has also been studied by using the two-gluon exchange model in Ref. [18]. However, their calculation method is very different from ours [1]. In their calculations, they separated their diagrams into two parts, and called one part the coherent diffractive contribution to the heavy quark production. However, this separation can not guarantee the gauge invariance [13]. In our approach, we follow the definition of Ref. [7], i.e., we call the process in which the whole Pomeron participants in the hard scattering process as the coherent diffractive process. Under this definition, all of the diagrams plotted in Fig.2 and Fig.3 for the partonic processes contribute to the coherent diffractive production.

The rest of the paper is organized as follows. In Sec.II, we will give the cross section formula for the partonic process in the leading order of perturbative QCD. In this section we employ the helicity amplitude method to calculate two partonic processes, $qp \to qgp$ and $gp \to ggp$. In Sec.III, we estimate the production rate of diffractive gluon jet at the Fermilab Tevatron by approximating the off-diagonal gluon distribution function by the usual diagonal gluon distribution function in the proton. We also compare the contributions from different partonic processes to the diffractive dijet production at the Tevatron. And the conclusions will be given in Sec.IV.

II. THE CROSS SECTION FORMULA FOR THE PARTONIC PROCESS

A. $qp \to qgp$ process

For the partonic process $qp \to qgp$, in the leading order of perturbative QCD, there are nine diagrams shown in Fig.2. The two-gluon system coupled to the proton (antiproton) in Fig.2 is in a color-singlet state, which characterizes the diffractive processes in perturbative QCD. Due to the positive signature of these diagrams (color-singlet exchange), we know

[1]For detailed discussions and comments, please see [13]

that the real part of the amplitude cancels out in the leading logarithmic approximation. To get the imaginary part of the amplitude, we must calculate the discontinuity represented by the crosses in each diagram of Fig.2.

The first four diagrams of Fig.2 are the same as those calculated in the diffractive direct photon production process at hadron colliders [16]. But, due to the existence of gluon-gluon interaction vertex in QCD, in the partonic process $qp \to qgp$, there are additional five diagrams (Fig.2(5)-(9)). These five diagrams are needed for a complete calculation in this order of QCD.

In our calculations, we express the formulas in terms of the Sudakov variables. That is, every four-momenta k_i are decomposed as,

$$k_i = \alpha_i q + \beta_i p + \vec{k}_{iT}, \tag{1}$$

where q and p are the momenta of the incident quark and the proton, $q^2 = 0$, $p^2 = 0$, and $2p \cdot q = W^2 = s$. Here s is the c.m. energy of the quark-proton system, i.e., the invariant mass of the partonic process $qp \to qgp$. α_i and β_i are the momentum fractions of q and p respectively. k_{iT} is the transverse momentum, which satisfies

$$k_{iT} \cdot q = 0, \quad k_{iT} \cdot p = 0. \tag{2}$$

All of the Sudakov variables for every momentum are determined by using the on-shell conditions of the momenta represented by the external lines and the crossed lines in the diagram. The calculations of these Sudakov variables are similar to those in the diffractive light quark jet production process $gp \to q\bar{q}p$ [14], and we can get the Sudakov variables of every momentum for the process $qp \to qgp$ from the relevant formulas of [14]. In the following, we list all of the Sudakov variables for the diffractive process $qp \to qgp$.

For the momentum u, we have

$$\alpha_u = 0, \quad \beta_u = x_{IP} = \frac{M_X^2}{s}, \quad u_T^2 = t = 0, \tag{3}$$

where M_X^2 is the invariant mass squared of the diffractive final state including the light quark and antiquark jets. For the high energy diffractive process, we know that $M_x^2 \ll s$, so we have β_u (x_{IP}) as a small parameter. For the momentum k,

$$\alpha_k(1 + \alpha_k) = -\frac{k_T^2}{M_X^2}, \quad \beta_k = -\alpha_k \beta_u, \tag{4}$$

where k_T is the transverse momentum of the out going quark jet. For the loop mentum l, because the results for β_l are not the same for the nine diagrams of Fig.2, we get its value from the formula of Ref. [14] for the relevant diagram. The results are

$$\begin{aligned}
\alpha_l &= -\frac{l_T^2}{s}, \\
\beta_l &= \frac{2(k_T, l_T) - l_T^2}{\alpha_k s}, \quad \text{for Diag.1, 2, 6,} \\
&= \frac{2(k_T, l_T) + l_T^2}{(1 + \alpha_k)s}, \quad \text{for Diag.5, 7, 8,} \\
&= -\frac{M_X^2 - l_T^2}{s}, \qquad \text{for Diag.3, 4, 9,}
\end{aligned} \tag{5}$$

where (k_T, l_T) is the 2-dimensional product of the transverse vectors $\vec{k}_T$ and $\vec{l}_T$.

Using these Sudakov variables, we can give the cross section formula for the partonic process $qp \to qgp$ as,

$$\frac{d\hat{\sigma}(qp \to qgp)}{dt}|_{t=0} = \frac{dM_X^2 d^2k_T d\alpha_k}{16\pi s^2 16\pi^3 M_X^2}\delta(\alpha_k(1+\alpha_k) + \frac{k_T^2}{M_X^2}) \sum \overline{|\mathcal{A}|}^2, \tag{6}$$

where $\mathcal{A}$ is the amplitude of the process $qp \to qgp$. We know that the real part of the amplitude $\mathcal{A}$ is zero, and the imaginary part of the amplitude $\mathcal{A}(qp \to qgp)$ for each diagram of Fig.2 has the following general form,

$$\mathrm{Im}\mathcal{A} = C_F(T^a_{ij}) \int \frac{d^2l_T}{(l_T^2)^2} F \times \bar{u}_i(u-k)\Gamma_\mu u_j(q), \tag{7}$$

where C_F is the color factor for each diagram. a is the color index of the incident gluon. Γ_μ represents some γ matrices including one propagator. F in the integral is defined as

$$F = \frac{3}{2s} g_s^3 f(x', x''; l_T^2), \tag{8}$$

where

$$f(x', x''; l_T^2) = \frac{\partial G(x', x''; l_T^2)}{\partial \ln l_T^2}, \tag{9}$$

where the function $G(x', x''; k_T^2)$ is the so-called off-diagonal gluon distribution function [11]. Here, x' and x'' are the momentum fractions of the proton carried by the two gluons. It is expected that at small x, there is no big difference between the off-diagonal and the usual diagonal gluon densities [19]. So, in the following calculations, we estimate the production rate by approximating the off-diagonal gluon density by the usual diagonal gluon density, $G(x', x''; Q^2) \approx xg(x, Q^2)$, where $x = x_{I\!P} = M_X^2/s$.

In [16], we calculate the cross section for the diffractive photon production process $qp \to \gamma qp$ by directly squaring the partonic process amplitude. However, in the calculations here for the partonic process $qp \to qgp$ because there are additional five diagrams contribution, it is not convenient to directly square the amplitude. Following Ref. [14], we calculate the amplitude by employing the *helicity amplitude* method [20,21]. Furthermore, we will show that by using the helicity amplitude method we can reproduce the cross section formula for the diffractive photon production process [16].

For the massless quark spinors, we define

$$u_\pm(p) = \frac{1}{\sqrt{2}}(1 \pm \gamma_5)u(p). \tag{10}$$

For the polarization vector of the outgoing gluon (its momentum is $k+q$), following the method of Ref. [21], we find that it is convenient to choose

$$\not{\epsilon}^{(\pm)} = N_e[(\not{k} + \not{q})\ \not{q}\ \not{p}(1 \mp \gamma_5) + \not{p}\ \not{q}(\not{k} + \not{q})(1 \pm \gamma_5)]. \tag{11}$$

The normalization factor N_e equals to

$$N_e = \frac{1}{s\sqrt{2k_T^2}}. \tag{12}$$

With this definition (11), we can easily get the scalar products between the four-momenta and the polarization vector e as

$$e\cdot p = 0, \quad e\cdot q = N_e\frac{k_T^2 s}{1+\alpha_k}, \quad e\cdot k_T = -N_e k_T^2 s, \quad e\cdot l_T = -N_e(k_T, l_T)s. \tag{13}$$

The helicity amplitudes for the processes in which the polarized Dirac particles are involved have the following general forms [20],

$$\bar{u}_\pm(p_f)Qu_\pm(p_i) = \frac{Tr[Q\ \not{p}_i\ \not{n}\ \not{p}_f(1\mp\gamma_5)]}{4\sqrt{(n\cdot p_i)(n\cdot p_f)}}, \tag{14}$$

where n is an arbitrary massless 4-vector, which is set to be $n = p$ in the following calculations. Using this formula (14), the calculations of the helicity amplitude $\mathcal{A}(\lambda_1, \lambda_2, \lambda_3)$ for the diffractive process $qp \to qgp$ is straightforward. Here λ_1 represents the helicity of the incident quark; λ_2 and λ_3 represent the helicities of the outgoing gluon and quark respectively. In our calculations, we only take the leading order contributions, and neglect the higher order contributions which are proportional to $\beta_u = \frac{M_X^2}{s}$ because in the high energy diffractive processes we have $\beta_u \ll 1$.

For the first four diagrams, to sum up together, the imaginary part of the amplitude $\mathcal{A}(+,+,+)$ is

$$\mathrm{Im}\mathcal{A}^{1234}(+,+,+) = \alpha_k^2(1+\alpha_k)\mathcal{N}\times\int\frac{d^2\vec{l}_T}{(l_T^2)^2}f(x', x''; l_T^2)(\frac{2}{9} - \frac{-1}{36}\frac{k_T^2 - (1+\alpha_k)(k_T, l_T)}{(\vec{k}_T - (1+\alpha_k)\vec{l}_T)^2}), \tag{15}$$

where $\frac{2}{9}$ and $\frac{-1}{36}$ are the color factors for Diags.1,4 and Diags.2,3 respectively, and $\mathcal{N}$ is defined as

$$\mathcal{N} = \frac{3s}{\sqrt{-2\alpha_k k_T^2}}g_s^3 T_{ij}^a. \tag{16}$$

The other helicity amplitudes for the first four diagrams have the similar forms as (15),

$$\begin{aligned}
&\mathrm{Im}\mathcal{A}^{1234}(-,-,-) = \mathrm{Im}\mathcal{A}^{1234}(+,+,+),\\
&\mathrm{Im}\mathcal{A}^{1234}(+,-,+) = \mathrm{Im}\mathcal{A}^{1234}(-,+,-) = \frac{-1}{\alpha_k}\mathrm{Im}\mathcal{A}^{1234}(+,+,+).
\end{aligned} \tag{17}$$

These amplitude expressions Eq. (15) can also serve as the calculations of the amplitude for the diffractive direct photon production process $qp \to q\gamma p$ [16] except the difference on the color factors.[2] In the direct photon process, the color factors for these four diagrams

[2]In Ref. [16], we did not employ the helicity amplitude method. If we use the amplitude expressions Eqs.(15) and (17) (correct the color factors) to calculate the photon production process $qp \to q\gamma p$, we can get the same result as that in [16]. This can be viewed as a cross check for the methods we used in the calculations.

are the same (they are all $\frac{2}{9}$). It is instructive to see what is the consequence of this difference. We know that the amplitude of the diffractive process in Eq. (7) must be zero in the limit $l_T^2 \to 0$. Otherwise, this will lead to a linear singularity when we perform the integration of the amplitude over l_T^2 due to existence of the factor $1/(l_T^2)^2$ in the integral of Eq. (7) [13]. This linear singularity is not proper in QCD calculations. So, we must first exam the amplitude behavior under the limit of $l_T^2 \to 0$ for all the diffractive processes in the calculations using the two-gluon exchange model. From Eq. (15), we can see that the amplitude for the diffractive direct photon production process $qp \to q\gamma p$ is exact zero at $l_T^2 \to 0$. However, for the process $qp \to qgp$ the amplitude for the first four diagrams is not exact zero in the limit $l_T^2 \to 0$ due to the inequality of the color factors between them. So, for this process there must be other diagrams in this order of perturbative QCD calculation to cancel out the linear singularity which rises from the first four diagrams. The last five diagrams of Fig.2 are just for this purpose.

Finally, by adding up all of the nine diagrams of Fig.2, the imaginary parts of the amplitudes are

$$\begin{aligned} \mathrm{Im}\mathcal{A}(+,+,+) &= \mathrm{Im}\mathcal{A}(-,-,-) = \frac{\alpha_k^2}{4}\mathcal{N}\times\mathcal{T}, \\ \mathrm{Im}\mathcal{A}(+,-,+) &= \mathrm{Im}\mathcal{A}(-,+,-) = -\frac{\alpha_k}{4}\mathcal{N}\times\mathcal{T}, \end{aligned} \tag{18}$$

where

$$\begin{aligned} \mathcal{T} = \int \frac{d^2\vec{l}_T}{(l_T^2)^2} f(x',x'';l_T^2)[&\frac{(1+\alpha_k)^2}{9}\frac{(k_T,l_T)-(1+\alpha_k)l_T^2}{(\vec{k}_T-(1+\alpha_k)\vec{l}_T)^2} - (1+\alpha_k)\frac{(k_T,l_T)+l_T^2}{(\vec{k}_T+\vec{l}_T)^2} \\ &-\alpha_k\frac{(k_T,l_T)-l_T^2}{(\vec{k}_T-\vec{l}_T)^2} + \alpha_k^2\frac{(k_T,l_T)-\alpha_k l_T^2}{(\vec{k}_T-\alpha_k\vec{l}_T)^2}]. \end{aligned} \tag{19}$$

From the above results, we can see that in the integration of the amplitude the linear singularity from different diagrams are canceled out by each other, which will guarantee there is no linear singularity in the total sum.

Another feature of the above results for the amplitudes is the relation to the differential off-diagonal gluon distribution function $f(x',x'';l_T^2)$. However, as mentioned above that there is no big difference between the off-diagonal gluon distribution function and the usual gluon distribution at small x, so we can simplify the integration of (19) by approximating the differential off-diagonal gluon distribution function $f(x',x'';l_T^2)$ by the usual diagonal differential gluon distribution function $f_g(x;l_T^2)$.

After integrating over the azimuth angle of $\vec{l}_T$, the integration $\mathcal{T}$ will then be

$$\begin{aligned} \mathcal{T} = \pi\int \frac{dl_T^2}{(l_T^2)^2} f_g(x;l_T^2)[&\frac{1+\alpha_k}{9}(\frac{1}{2}-\frac{k_T^2-(1+\alpha_k)l_T^2}{2|k_T^2-(1+\alpha_k)l_T^2|}) + (\frac{1}{2}-\frac{k_T^2-l_T^2}{2|k_T^2-l_T^2|}) \\ &+\alpha_k(\frac{1}{2}-\frac{k_T^2-\alpha_k l_T^2}{2|k_T^2-\alpha_k l_T^2|})]. \end{aligned} \tag{20}$$

In the above integration, if $l_t^2 < k_T^2/(1+\alpha_k)^2$ the first term of the integration over l_T^2 will be zero; if $l_t^2 < k_T^2$ the second term will be zero; if $l_t^2 < k_T^2/\alpha_k^2$ the third term will be zero. So, the dominant regions contributing to the three integration terms are $l_t^2 \sim k_T^2/(1+\alpha_k)^2$,

$l_t^2 \sim k_T^2$, and $l_t^2 \sim k_T^2/\alpha_k^2$ respectively. Approximately, by ignoring some evolution effects of the differential gluon distribution function $f_g(x; l_T^2)$ in the above dominant integration regions, we get the following results for the integration $\mathcal{T}$,

$$\mathcal{T} = \frac{\pi}{k_T^2}[f_g(x; k_T^2) + \frac{(1+\alpha_k)^3}{9} f_g(x; \frac{k_T^2}{(1+\alpha_k)^2}) + \alpha_k^3 f_g(x; \frac{k_T^2}{\alpha_k^2})]. \tag{21}$$

Obtained the formula for the integration $\mathcal{T}$, the amplitude squared for the partonic process $qp \to qgp$ will be reduced to, after averaging over the spin and color degrees of freedom,

$$\overline{|\mathcal{A}|}^2 = \frac{\alpha_s^3 (4\pi)^3}{24} \frac{1+\alpha_k^2}{M_X^2(1+\alpha_k)} s^2 |\mathcal{T}|^2. \tag{22}$$

And the cross section for the partonic process $qp \to qgp$ is

$$\frac{d\hat{\sigma}(qp \to qgp)}{dt}|_{t=0} = \int_{M_X^4 > 4k_T^2} dM_X^2 dk_T^2 d\alpha_k [\delta(\alpha_k - \alpha_1) + \delta(\alpha_k - \alpha_2)] \frac{\alpha_s^3}{96(M_X^2)^2} \frac{1+\alpha_K^2}{1+\alpha_k} \frac{1}{\sqrt{1 - \frac{4k_T^2}{M_X^2}}} |\mathcal{T}|^2, \tag{23}$$

where $\alpha_{1,2}$ are the solutions of the following equations,

$$\alpha(1+\alpha) + \frac{k_T^2}{M_X^2} = 0. \tag{24}$$

The integral bound $M_X^2 > 4k_T^2$ in (23) shows that the dominant contribution of the integration over M_X^2 comes from the region of $M_X^2 \sim 4k_T^2$. Using Eq. (4), this indicates that in this dominant region α_k is of order of 1. So, in the integration $\mathcal{T}$ the differential gluon distribution function $f_g(x; Q^2)$ of the three terms can approximately take their values at the same scale of $Q^2 = k_T^2$. That is, the integration $\mathcal{T}$ is then simplified to

$$\mathcal{T} = \frac{\pi}{9k_T^2} f_g(x; k_T^2)(1+\alpha_k)(10 - 7\alpha_k + 10\alpha_k^2). \tag{25}$$

Numerical calculations show that there is little difference between the cross sections by using these two different parametrizations of $\mathcal{T}$, Eq. (21) and Eq. (25). So, in Sec.IV, we use Eqs. (23) and (25) to estimate the diffractive production rate at the Fermilab Tevatron.

B. $gp \to ggp$ process

For the partonic process $gp \to ggp$, there are twelve diagrams in the leading order contributions as shown in Fig.3. The first nine diagrams are due to the existence of the three-gluon interaction vertex, and the last three diagrams are due to the existence of the four-gluon interaction vertex. But it will be shown in the following calculations, the last three diagrams do not contribute under some choice of the polarizations of the three external gluons.

The Sudakov variables can be calculated by the similar method used in the last subsection. And those Sudakov variables of the momenta u, k for the process $gp \to ggp$ are the same as those in the last subsection. For the loop momentum l, the relevant Sudakov variables for each diagram are

$$\begin{aligned}
\alpha_l &= -\frac{l_T^2}{s}, \\
\beta_l &= \frac{2(k_T, l_T) - l_T^2}{\alpha_k s}, \quad \text{for Diag.1, 4, 6, 10,} \\
&= \frac{2(k_T, l_T) + l_T^2}{(1+\alpha_k)s}, \quad \text{for Diag.2, 3, 5, 11,} \\
&= -\frac{M_X^2 - l_T^2}{s}, \qquad \text{for Diag.7, 8, 9, 12.}
\end{aligned} \tag{26}$$

And also, we can express the cross section formula for the partonic process $gp \to ggp$ in the following form,

$$\frac{d\hat{\sigma}(gp \to ggp)}{dt}|_{t=0} = \frac{dM_X^2 d^2k_T d\alpha_k}{16\pi s^2 16\pi^3 M_X^2} \delta(\alpha_k(1+\alpha_k) + \frac{k_T^2}{M_X^2}) \sum \overline{|\mathcal{A}|}^2, \tag{27}$$

where $\mathcal{A}$ is the amplitude of the process $gp \to ggp$. We know that the real part of the amplitude $\mathcal{A}$ is zero, and the imaginary part of the amplitude $\mathcal{A}(gp \to ggp)$ for each diagram of Fig.3 has the following general form,

$$\mathrm{Im}\mathcal{A} = C_F f_{abc} \int \frac{d^2 l_T}{(l_T^2)^2} G(e_1, e_2, e_3) \times F, \tag{28}$$

where C_F is the color factor for each diagram. $a,\ b,\ c$ are the color indexes for the incident gluon and the two outgoing gluons respectively, and f_{abc} are the antisymmetric $SU(3)$ structure constants. $G(e_1, e_2, e_3)$ represents the interaction part including one propagator for the first nine diagrams, where $e_1,\ e_2,\ e_3$ are the polarization vectors for the incident gluon and the two outgoing gluons. F in the integral is the same as that in Eq.(8).

The color factors C_F for the twelve diagrams are

$$\begin{aligned}
C_F &= \frac{1}{2}, \qquad \text{for Diag.1, 7,} \\
C_F &= -\frac{1}{2}, \qquad \text{for Diag.2,} \\
C_F &= -\frac{1}{4}, \qquad \text{for Diag.3, 6, 9,} \\
C_F &= \frac{1}{4}, \qquad \text{for Diag.4, 5, 8,} \\
C_F &= \frac{3}{4}, \qquad \text{for Diag.10, 11, 12.}
\end{aligned} \tag{29}$$

Following the calculation method used in the last subsection, we employ the helicity amplitude method to calculate the amplitude Eq.(28). For the polarization vector of the incident gluon, which is transversely polarized, we choose,

$$e_1^{(\pm)} = \frac{1}{\sqrt{2}}(0, 1, \pm i, 0). \tag{30}$$

For the two outgoing gluons, we choose their polarization vectors as [21]

$$\begin{aligned} \not{e}_2^{(\pm)} &= N_e[(\not{k}+ \not{q})\ \not{q}\ \not{p}(1 \mp \gamma_5)+ \not{p}\ \not{q}(\not{k}+ \not{q})(1 \pm \gamma_5)], \\ \not{e}_3^{(\pm)} &= N_e[(\not{n}- \not{k})\ \not{q}\ \not{p}(1 \mp \gamma_5)+ \not{p}\ \not{q}(\not{n}- \not{k})(1 \pm \gamma_5)]. \end{aligned} \tag{31}$$

The normalization factor N_e has the same form as in Eq.(12). Under the above choice of the polarization vectors for the external gluons, we can easily find that they are satisfied the following equations,

$$p \cdot e_1 = p \cdot e_2 = p \cdot e_3 = 0. \tag{32}$$

With these relations, we can further find that the last three diagrams do not contribute to the partonic process $gp \to ggp$.

For the first nine diagrams, there are two helicity amplitudes among the eight helicity amplitudes do not contribute in the context of the above choice of the polarizations of the external gluons, i.e.,

$$\mathrm{Im}\mathcal{A}(+,+,+) = \mathrm{Im}\mathcal{A}(-,-,-) = 0. \tag{33}$$

In the expression of the amplitude $\mathcal{A}(\lambda(e_1), \lambda(e_2), \lambda(e_3))$, λ denote the helicities for the three gluons respectively. The other six helicity amplitudes are divided into the following three different sets,

$$\begin{aligned} &\mathrm{Im}\mathcal{A}(+,-,-) \sim \mathrm{Im}\mathcal{A}(-,+,+), \\ &\mathrm{Im}\mathcal{A}(+,-,+) \sim \mathrm{Im}\mathcal{A}(-,+,-), \\ &\mathrm{Im}\mathcal{A}(+,+,-) \sim \mathrm{Im}\mathcal{A}(-,-,+). \end{aligned} \tag{34}$$

For the first helicity amplitudes set, $\mathrm{Im}\mathcal{A}(\pm,\mp,\mp)$, to sum up all of the nine diagrams, we get

$$\mathrm{Im}\mathcal{A}(\pm,\mp,\mp) = \mathcal{N}'\pi e_1^{(\pm)} \cdot k_T \mathcal{I}, \tag{35}$$

where $\mathcal{N}'$ is defined as

$$\mathcal{N}' = \frac{3}{4}\frac{s}{k_T^2} g_s^3 f_{abc}. \tag{36}$$

And the integration $\mathcal{I}$ is

$$\begin{aligned} \mathcal{I} = &\frac{1}{\pi}\int \frac{d^2\vec{l}_T}{(l_T^2)^2} f(x', x''; l_T^2)[-(1+\alpha_k)\frac{k_T^2 + (k_T, l_T)}{(\vec{k}_T + \vec{l}_T)^2} + \alpha_k \frac{k_T^2 - (k_T, l_T)}{(\vec{k}_T - \vec{l}_T)^2} \\ &+(1+\alpha_k)^2 \frac{k_T^2 - (1+\alpha_k)(k_T, l_T)}{(\vec{k}_T - (1+\alpha_k)\vec{l}_T)^2} - \alpha_k^2 \frac{k_T^2 - \alpha_k(k_T, l_T)}{(\vec{k}_T - \alpha_k \vec{l}_T)^2}] \end{aligned} \tag{37}$$

$$\begin{aligned} = &\frac{1}{\pi}\int \frac{d^2\vec{l}_T}{(l_T^2)^2} f(x', x''; l_T^2)[(1+\alpha_k)\frac{(k_T, l_T) + l_T^2}{(\vec{k}_T + \vec{l}_T)^2} + \alpha_k \frac{(k_T, l_T) - l_T^2}{(\vec{k}_T - \vec{l}_T)^2} \\ &-(1+\alpha_k)^2 \frac{(k_T, l_T) - (1+\alpha_k) l_T^2}{(\vec{k}_T - (1+\alpha_k)\vec{l}_T)^2} + \alpha_k^2 \frac{(k_T, l_T) - \alpha_k l_T^2}{(\vec{k}_T - \alpha_k \vec{l}_T)^2}]. \end{aligned} \tag{38}$$

From the above equations, we can check that there is no linear singularity at the limit of $l_T^2 \to 0$ in the integration of the amplitude over the loop momentum. The first term of the integration $\mathcal{I}$ in Eq.(37) comes from the contribution of Diag.3; the second term comes from Diag.4; the third term comes from Diag.6 and Diag.9; the last term comes from Diag.5 and Diag.8. The contributions from Diags.1, 2 and 7 are canceled out by each other. From (37), we can see that the linear singularities coming from the four terms are canceled out by each other. The final result for the amplitude is now free of linear singularity. We must emphasize here that only the total sum of the contributions from all of the diagrams is free of linear singularity. The separation of these diagrams will cause linear singularity.

Following the argument in the last subsection of the calculation for the partonic process $qp \to qgp$, we can approximate the differential off-diagonal gluon distribution function $f(x', x''; l_T^2)$ by the usual diagonal differential gluon distribution function $f_g(x; l_T^2)$ to further simplify the integration of $\mathcal{I}$. After integrating over the azimuth angle of $\vec{l}_T$, this integration will then be

$$\mathcal{I} = \int \frac{dl_T^2}{(l_T^2)^2} f_g(x; l_T^2)[(\frac{1}{2} - \frac{k_T^2 - l_T^2}{2|k_T^2 - l_T^2|}) - (1+\alpha_k)(\frac{1}{2} - \frac{k_T^2 - (1+\alpha_k)l_T^2}{2|k_T^2 - (1+\alpha_k)l_T^2|}) + \alpha_k(\frac{1}{2} - \frac{k_T^2 - \alpha_k l_T^2}{2|k_T^2 - \alpha_k l_T^2|})]. \tag{39}$$

The above equation shows that the integration $\mathcal{I}$ here has the similar behavior as that of the integration $\mathcal{T}$ of Eq.(20) in the last subsection. So, the three terms of the above integration $\mathcal{I}$ are dominantly contributed from the integral regions of l_T^2 as $l_t^2 \sim k_T^2/(1+\alpha_k)^2$, $l_t^2 \sim k_T^2$, and $l_t^2 \sim k_T^2/\alpha_k^2$ respectively. Approximately, we may also ignore the evolution effects of the differential gluon distribution function $f_g(x; l_T^2)$ in the above dominant integration regions, and so the integration $\mathcal{I}$ is reduced to

$$\mathcal{I} = \frac{1}{k_T^2}[f_g(x; k_T^2) - (1+\alpha_k)^3 f_g(x; \frac{k_T^2}{(1+\alpha_k)^2}) + \alpha_k^3 f_g(x; \frac{k_T^2}{\alpha_k^2})]. \tag{40}$$

For the second helicity amplitudes set, $\mathrm{Im}\mathcal{A}(\pm, \mp, \pm)$, the calculations are more complicated, and the contribution from Diag.3 is

$$\mathrm{Im}\mathcal{A}^3(\pm, \mp, \pm) = -\mathcal{N}'(1+\alpha_k)^2 \int \frac{d^2\vec{l}_T}{(l_T^2)^2} f(x', x''; l_T^2) \frac{\alpha_k k_T^2 \vec{e}_1^{(\pm)} \cdot (\vec{k}_T + \vec{l}_T) + (k_T^2 + (k_T, l_T))\vec{e}_1^{(\pm)} \cdot \vec{k}_T}{(\vec{k}_T + \vec{l}_T)^2}. \tag{41}$$

The contribution from Diag.4 is

$$\mathrm{Im}\mathcal{A}^4(\pm, \mp, \pm) = \mathcal{N}'\alpha_k(1+\alpha_k) \int \frac{d^2\vec{l}_T}{(l_T^2)^2} f(x', x''; l_T^2) \frac{\alpha_k k_T^2 \vec{e}_1^{(\pm)} \cdot (\vec{k}_T - \vec{l}_T) + (k_T^2 - (k_T, l_T))\vec{e}_1^{(\pm)} \cdot \vec{k}_T}{(\vec{k}_T - \vec{l}_T)^2}. \tag{42}$$

The contributions from Diag.5 and Diag.8, to sum up together, are

$$\mathrm{Im}\mathcal{A}^{58}(\pm,\mp,\pm) = -\mathcal{N}'\alpha_k(1+\alpha_k)\int\frac{d^2\vec{l}_T}{(l_T^2)^2}f(x',x'';l_T^2)$$
$$\frac{\alpha_k k_T^2\vec{e}_1^{(\pm)}\cdot(\vec{k}_T-\alpha_k\vec{l}_T)+(k_T^2-\alpha_k(k_T,l_T))\vec{e}_1^{(\pm)}\cdot\vec{k}_T}{(\vec{k}_T-\alpha_k\vec{l}_T)^2}. \tag{43}$$

The contributions from Diag.6 and Diag.9, to sum up together, are

$$\mathrm{Im}\mathcal{A}^{69}(\pm,\mp,\pm) = \mathcal{N}'(1+\alpha_k)^2\int\frac{d^2\vec{l}_T}{(l_T^2)^2}f(x',x'';l_T^2)$$
$$\frac{\alpha_k k_T^2\vec{e}_1^{(\pm)}\cdot(\vec{k}_T-(1+\alpha_k)\vec{l}_T)+(k_T^2-(1+\alpha_k)(k_T,l_T))\vec{e}_1^{(\pm)}\cdot\vec{k}_T}{(\vec{k}_T-(1+\alpha_k)\vec{l}_T)^2}. \tag{44}$$

The contributions from other three diagrams (Diag.1, Diag.2 and Diag.7) are canceled out by each other. From the above results Eqs.(41-44), we can see that every term has linear singularity at the limit of $l_T^2\to 0$ in the integration of the amplitude over l_T^2, while their total sum is free of the linear singularity.

Following the procedure as we do for the helicity amplitude $\mathcal{A}(\pm,\mp,\mp)$ in the above, we can approximate the off-diagonal gluon distribution function $f(x',x'';l_T^2)$ by the usual diagonal differential gluon distribution function $f_g(x;l_T^2)$. After integrating over the azimuth angle of $\vec{l}_T$, to sum up all of Eqs.(41-44), we get the helicity amplitude,

$$\mathrm{Im}\mathcal{A}(\pm,\mp,\pm) = \mathcal{N}'\pi(1+\alpha_k)^2\vec{e}_1^{(\pm)}\cdot k_T\mathcal{I}, \tag{45}$$

where $\mathcal{I}$ is the same as Eq.(39) and then Eq.(40) under the same approximation.

For the third helicity amplitudes set, $\mathrm{Im}\mathcal{A}(\pm,\pm,\mp)$, the calculations are similar to the calculations of $\mathrm{Im}\mathcal{A}(\pm,\mp,\pm)$. The contribution from Diag.3 is

$$\mathrm{Im}\mathcal{A}^{3}(\pm,\pm,\mp) = -\mathcal{N}'\alpha_k(1+\alpha_k)\int\frac{d^2\vec{l}_T}{(l_T^2)^2}f(x',x'';l_T^2)$$
$$\frac{(1+\alpha_k)k_T^2\vec{e}_1^{(\pm)}\cdot(\vec{k}_T+\vec{l}_T)-(k_T^2+(k_T,l_T))\vec{e}_1^{(\pm)}\cdot\vec{k}_T}{(\vec{k}_T+\vec{l}_T)^2}. \tag{46}$$

The contribution from Diag.4 is

$$\mathrm{Im}\mathcal{A}^{4}(\pm,\pm,\mp) = \mathcal{N}'\alpha_k^2\int\frac{d^2\vec{l}_T}{(l_T^2)^2}f(x',x'';l_T^2)$$
$$\frac{(1+\alpha_k)k_T^2\vec{e}_1^{(\pm)}\cdot(\vec{k}_T-\vec{l}_T)-(k_T^2-(k_T,l_T))\vec{e}_1^{(\pm)}\cdot\vec{k}_T}{(\vec{k}_T-\vec{l}_T)^2}. \tag{47}$$

The contributions from Diag.5 and Diag.8, to sum up together, are

$$\mathrm{Im}\mathcal{A}^{58}(\pm,\pm,\mp) = -\mathcal{N}'\alpha_k^2\int\frac{d^2\vec{l}_T}{(l_T^2)^2}f(x',x'';l_T^2)$$
$$\frac{(1+\alpha_k)k_T^2\vec{e}_1^{(\pm)}\cdot(\vec{k}_T-\alpha_k\vec{l}_T)-(k_T^2-\alpha_k(k_T,l_T))\vec{e}_1^{(\pm)}\cdot\vec{k}_T}{(\vec{k}_T-\alpha_k\vec{l}_T)^2}. \tag{48}$$

The contributions from Diag.6 and Diag.9, to sum up together, are

$$\mathrm{Im}\mathcal{A}^{69}(\pm,\pm,\mp) = \mathcal{N}'\alpha_k(1+\alpha_k)\int \frac{d^2\vec{l}_T}{(l_T^2)^2} f(x',x'';l_T^2) \\ \frac{(1+\alpha_k)k_T^2\vec{e}_1^{(\pm)}\cdot(\vec{k}_T-(1+\alpha_k)\vec{l}_T)-(k_T^2-(1+\alpha_k)(k_T,l_T))\vec{e}_1^{(\pm)}\cdot\vec{k}_T}{(\vec{k}_T-(1+\alpha_k)\vec{l}_T)^2}. \quad (49)$$

And also, we find that the contributions from other three diagrams (Diag.1, Diag.2 and Diag.7) are canceled out by each other, and the total sum of Eqs.(46-49) is free of the linear singularity. If we approximate the off-diagonal gluon distribution function $f(x',x'';l_T^2)$ by the usual diagonal differential gluon distribution function $f_g(x;l_T^2)$, and integrate over the azimuth angle of $\vec{l}_T$, their sum will lead to a similar result as in Eq.(45),

$$\mathrm{Im}\mathcal{A}(\pm,\pm,\mp) = \mathcal{N}'\pi\alpha_k^2\vec{e}_1^{(\pm)}\cdot k_T\mathcal{I}. \quad (50)$$

By summing up all of the helicity amplitudes Eqs.(35), (45) and 50), we will get the amplitude squared for the partonic process $gp \to ggp$, after averaging over the spin and color degrees of freedom,

$$\overline{|\mathcal{A}|}^2 = \frac{27\pi^2\alpha_s^3(4\pi)^3}{16}\frac{s^2}{k_t^2}(1-\frac{k_T^2}{M_X^2})^2|\mathcal{I}|^2. \quad (51)$$

And the cross section for the partonic process $gp \to ggp$ is

$$\frac{d\hat{\sigma}(gp\to ggp)}{dt}|_{t=0} = \int_{M_X^4>4k_T^2} dM_X^2dk_T^2\frac{27\alpha_s^3\pi^2}{32M_X^2k_T^2}(1-\frac{k_T^2}{M_X^2})^2|\mathcal{I}|^2\frac{1}{\sqrt{1-\frac{4k_T^2}{M_X^2}}}, \quad (52)$$

Following the same argument in the last subsection for the calculations of the partonic process $qp \to qgp$, we see that the dominant contribution of the integration over M_X^2 comes from the region of $M_X^2 \sim 4k_T^2$, where the differential gluon distribution function $f_g(x;Q^2)$ of the three terms in the integration $\mathcal{I}$ can approximately take their values at the same scale of $Q^2 = k_T^2$. That is, the integration $\mathcal{I}$ is then simplified to

$$\mathcal{I} = \frac{1}{k_T^2}(-3\alpha_k(1+\alpha_k))f_g(x;k_T^2) = \frac{1}{k_T^2}\frac{3k_T^2}{M_X^2}f_g(x;k_T^2) = \frac{3}{M_X^2}f_g(x;k_T^2). \quad (53)$$

III. NUMERICAL RESULTS

In this section we study the numerical behavior of the diffractive gluon jet production at the Fermilab Tevatron. We will study the p_T distribution and x_1 distribution of the cross section. We will also compare the gluon jet production with the quark jet production which has been calculated in [13,14]. A more thorough phenomenological study, including a comparison to currently available data at Tevatron on the diffractive dijet production rate, will be presented elsewhere.

Provided with the cross section formulas for the partonic processes $qp \to qgp$ (23) and $gp \to ggp$ (52), we can calculate the cross section of the diffractive gluon jet production at hadron level. However, as mentioned above, there exists nonfactorization effect caused by the spectator interactions in the hard diffractive processes in hadron collisions. Here, we use a suppression factor $\mathcal{F}_S$ to describe this nonfactorization effect in the hard diffractive processes at hadron colliders [8,10]. At the Tevatron, the value of $\mathcal{F}_S$ may be as small as $\mathcal{F}_S \approx 0.1$ [8,9]. That is to say, the total cross section of the diffractive processes at the Tevatron may be reduced down by an order of magnitude due to this nonfactorization effect. In the following numerical calculations, we adopt this suppression factor value to evaluate the diffractive production rate.

In our calculations, the scales for the parton distribution functions and the running coupling constant are both set to be $Q^2 = k_T^2$. For the parton distribution functions, we choose the GRV NLO set [22].

In Fig.4, we plot the differential cross section $d\sigma/dt|_{t=0}$ as a function of the lower bound of the transverse momentum of the gluon jet, $k_{T\min}$. This figure shows that the cross section is sensitive to the transverse momentum cut $k_{T\min}$. We plot separately the contributions from the two subprocesses, $qp \to qgp$ and $gp \to ggp$. By comparison, we also plot the cross section of the diffractive light quark jet production calculated in [14]. The three curves in this figure show that the contribution from the subprocess $gp \to ggp$ is two orders of magnitude larger than that from the subprocess $qp \to qgp$ for the diffractive gluon jet production, and the light quark jet production rate is in the same order with that of the subprocess $qp \to qgp$. This indicates that the diffractive dijet production at hadron colliders dominantly comes from the subprocess $gp \to ggp$ in the two-gluon exchange model.

In Fig.5, we plot the differential cross section $d\sigma/dt|_{t=0}$ as a function of the lower bound of the momentum fraction of the proton carried by the incident gluon $x_{1\min}$, where we set $k_{T\min} = 5\ GeV$. Fig.5(a) is for the contribution from the subprocess $qp \to qgp$, and Fig.5(b) is from the subprocess $gp \to ggp$. These two figures show that the dominant contribution comes from the region of $x_1 \sim 10^{-2} - 10^{-1}$ for the subprocess $gp \to ggp$, and $x_1 > 10^{-1}$ for the subprocess $qp \to qgp$. These properties are similar to those of the diffractive charm jet and W boson productions calculated in [13,15].

IV. CONCLUSIONS

In this paper, we have calculated the diffractive gluon jet production at hadron colliders in perturbative QCD by using the two-gluon exchange model. We find that the production cross section is related to the squared of the differential gluon distribution function $\partial G(x;Q^2)/\partial ln Q^2$ at the scale of $Q^2 \sim k_T^2$, where k_T is the transverse momentum of the final state gluon jet. We have also compared the production rate of the gluon jet in the diffractive processes with those of the light quark jet and heavy quark jet productions, and found that the production rates of these processes are in the same order of magnitude.

As we know, the large transverse momentum dijet production in the diffractive processes at hadron colliders is important to study the diffractive mechanism and the nature of the Pomeron. The CDF collaboration at the Fermilab Tevatron have reported some results on this process [9]. Up to now, we have calculated all of the dijet production subprocesses in the diffractive processes at hadron colliders, including $gp \to q\bar{q}p$, $qp \to qgp$ and $gp \to ggp$

processes. In a forthcoming paper, we will compare the available data on the diffractive dijet production cross section at the Tevatron [9] to the predictions of our model to test the validity of perturbative QCD description of the diffractive processes at hadron colliders.

ACKNOWLEDGMENTS

This work was supported in part by the National Natural Science Foundation of China, the State Education Commission of China, and the State Commission of Science and Technology of China.

REFERENCES

[1] P.D.B. Collins, *An introduction to Regge theory and high energy physics*, Cambridge University Press, Cambridge (1977).

[2] M.G. Ryskin, Z. Phys. **C37**, 89 (1993); M.G. Ryskin, et al., Z. Phys. **C76**, 231 (1996).

[3] S.J. Brodsky et al., Phys. Rev. **D50**, 3134 (1994); L. Frankfurt et al., Phys. Rev. **D57**, 512 (1998).

[4] T. Gehrmann and W.J. Stitling, Z. Phys. **C70**, 69 (1996); M. Genovese et al., Phys. Lett. **B378**, 347 (1996); E.M. Levin et al., hep-ph/9606443.

[5] M. Derrick et al, ZEUS collaboration, Phys. Lett. **B350** 120 (1995); S. Aid et. al., H1 Collaboration, Nucl. Phys. B **472**, 3 (1996).

[6] P.V. Landshoff and J.C. Polkinghorne, Nucl. Phys. **B33**, 221 (1971), **B36**, 642 (1972); F. Henyey and R. Savit, Phys. Lett. **B52**, 71 (1974); J.L. Cardy and G.A. Winbow, Phys. Lett. **B52**, 95 (1974); C. DeTar, S.D. Ellis and P.V. Landshoff, Nucl. Phys. **B87**, 176 (1975).

[7] J.C. Collins, L. Frankfurt and M. Strikman, Phys. Lett. **B307**, 161 (1993);

[8] D.E. Soper, talk at DIS97 conference, Chicago, April 1997, hep-ph/9707384.

[9] F. Abe et al., Phys. Rev. Lett. **78**, 2698 (1997); F. Abe et al., Phys. Rev. Lett. **79**, 2636 (1997).

[10] J.D.Bjorken, Phys. Rev. **D45** 4077 (1992); **D47** 10 (1993); E.Gotsman,E. Levin and U. Maor, Phys. Lett. **B309** 199 (1993); Nucl. Phys. **B493** 354 (1997); hep-ph/9804404; R.S.Fletcher, Phys. Rev. **D48** 5162 (1993). A.D. Martin, M.G. Ryskin and V.A. Khoze, Phys. Rev. **D56** 5867 (1997).

[11] X. Ji, Phys. Rev. Lett. **78**, 610 (1997), Phys. Rev. **D55**, 7114 (1997); A.V. Radyushkin, Phys. Lett. **B385**, 333 (1996), Phys. Lett. **B380**, 417 (1996), Phys. Rev. **D56**, 5524 (1997).

[12] F. Yuan, J.S. Xu, H.A. Peng, and K.T. Chao, Phys. Rev. **D58**, 114016 (1998).

[13] F. Yuan and K.T. Chao, hep-ph/9810340, to appear in Phys. Rev. **D**.

[14] F. Yuan and K.T. Chao, PKU-TP-98-53, hep-ph/9904237.

[15] F. Yuan and K.T. Chao, hep-ph/9811285.

[16] F. Yuan and K.T. Chao, PKU-TP-98-54, hep-ph/9904238.

[17] N.N. Nikolaev and B.G. Zakharov, Phys. Lett. **B332**, 177 (1994); K. Golec-Biernat, J. Kwiecinski, and A.D. Martin, Preprint DTP/98/12.

[18] G. Alves, E. Levin, and A. Santoro, Phys. Rev. **D55**, 2683 (1997).

[19] P. Hoodbhoy, Phys. Rev. **D56**, 388 (1997); L. Frankfurt et al., Phys. Lett. **B418**, 345 (1998); A.D. Martin and M.G. Ryskin, Phys. Rev. **D57**, 6692 (1998).

[20] A. L. Bondarev, hep-ph/9710398, and references therein.

[21] P.De Causmaecker, R.Gastmans, W.Troost, T.T.Wu, Phys. Lett. **B105**, 215 (1981), Nucl. Phys. **B206**, 53 (1982); R.Gastmans, W.Troost, T.T.Wu, Nucl. Phys. **B291**, 731 (1987).

[22] M. Glück et al. Z. Phys. **C67**, 433 (1995).

Figure Captions

Fig.1. Sketch diagram for the diffractive dijet production at hadron colliders in perturbative QCD. The final state jet lines represent the outgoing quark or gluon lines, and the incident parton from the upper proton (labeled by $x_1 p_1$) can be quark or gluon correspondingly.
Fig.2. The lowest order perturbative QCD diagrams for partonic process $qp \to qgp$.
Fig.3. The lowest order perturbative QCD diagrams for partonic process $gp \to ggp$.
Fig.4. The differential cross section $d\sigma/dt|_{t=0}$ for the gluon jet production in the diffractive processes as a function of $k_{T\min}$ at the Fermilab Tevatron, where $k_{T\min}$ is the lower bound of the transverse momentum of the out going gluon jet.
Fig.5. The differential cross section $d\sigma/dt|_{t=0}$ for the gluon jet production as a function of $x_{1\min}$, where $x_{1\min}$ is the lower bound of x_1 in the integration of the cross section. (a) is for the contribution from the subprocess $qp \to qgp$, and (b) is from the subprocess $gp \to ggp$.

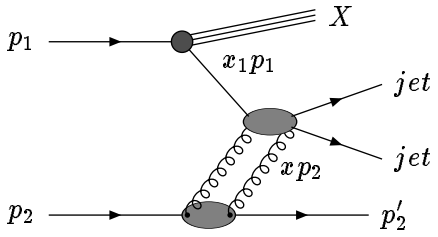

Fig.1

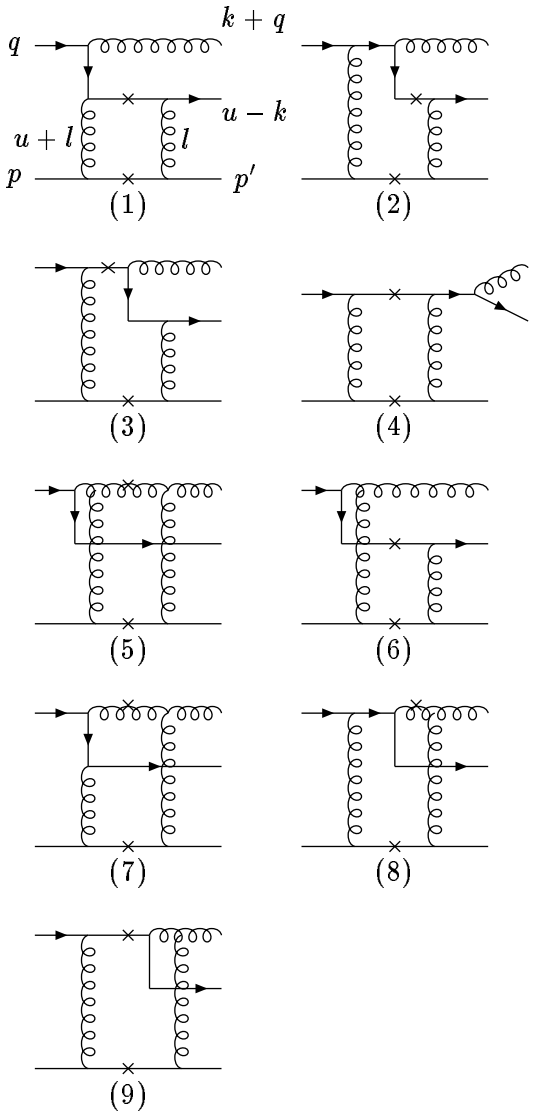

Fig.2

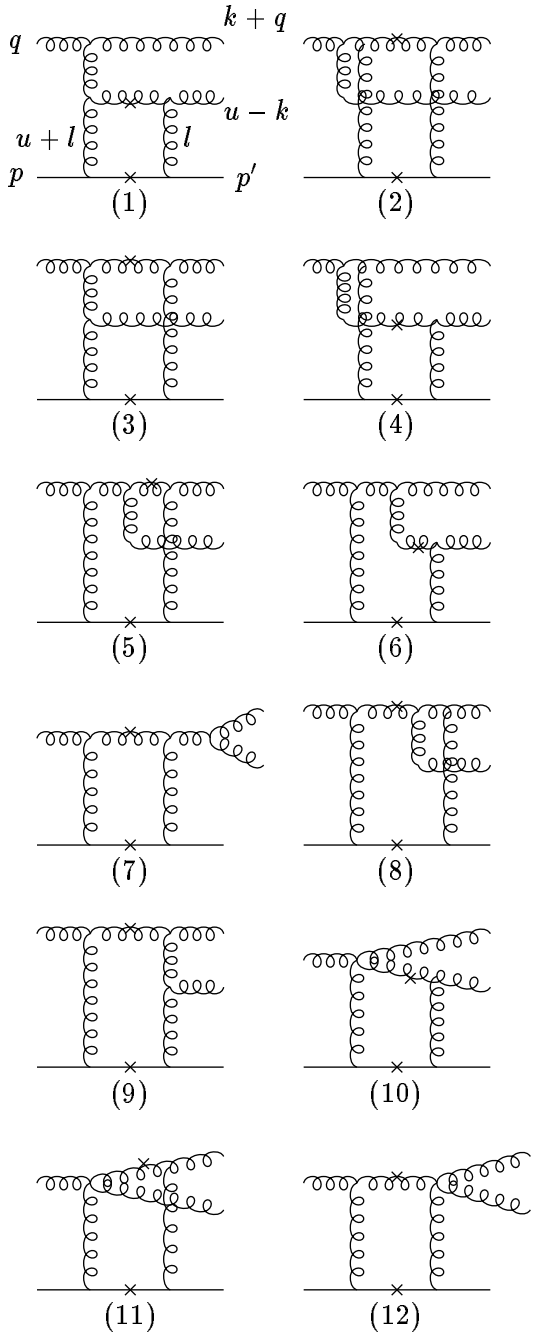

Fig.3

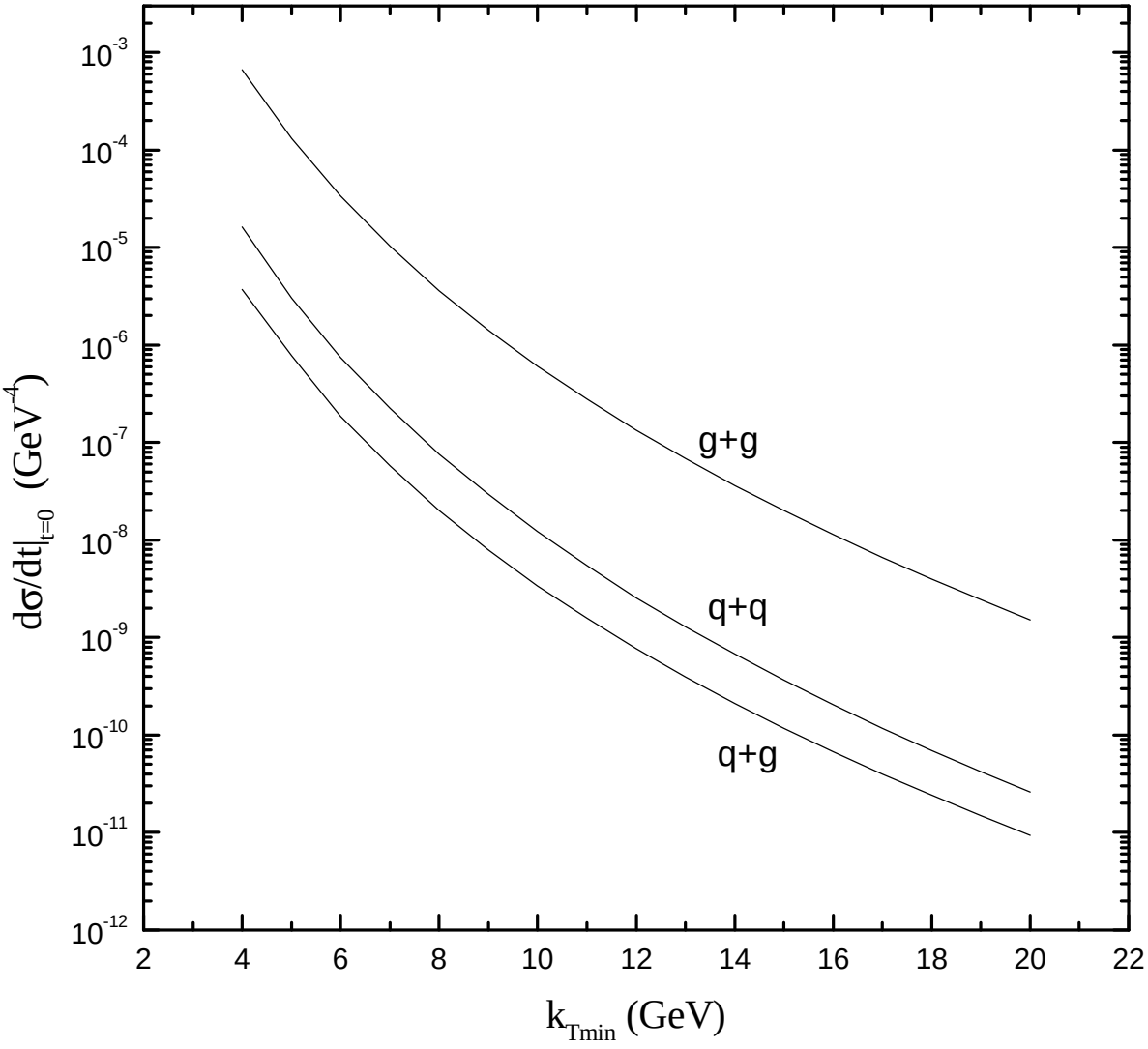
10^{-3}
10^{-4}
10^{-5}
10^{-6}
10^{-7}
10^{-8}
10^{-9}
10^{-10}
10^{-11}
10^{-12}
$d\sigma/dt|_{t=0}$ (GeV^{-4})
g+g
q+q
q+g
2
4
6
8
10
12
14
16
18
20
22
k_{Tmin} (GeV)

Fig.4

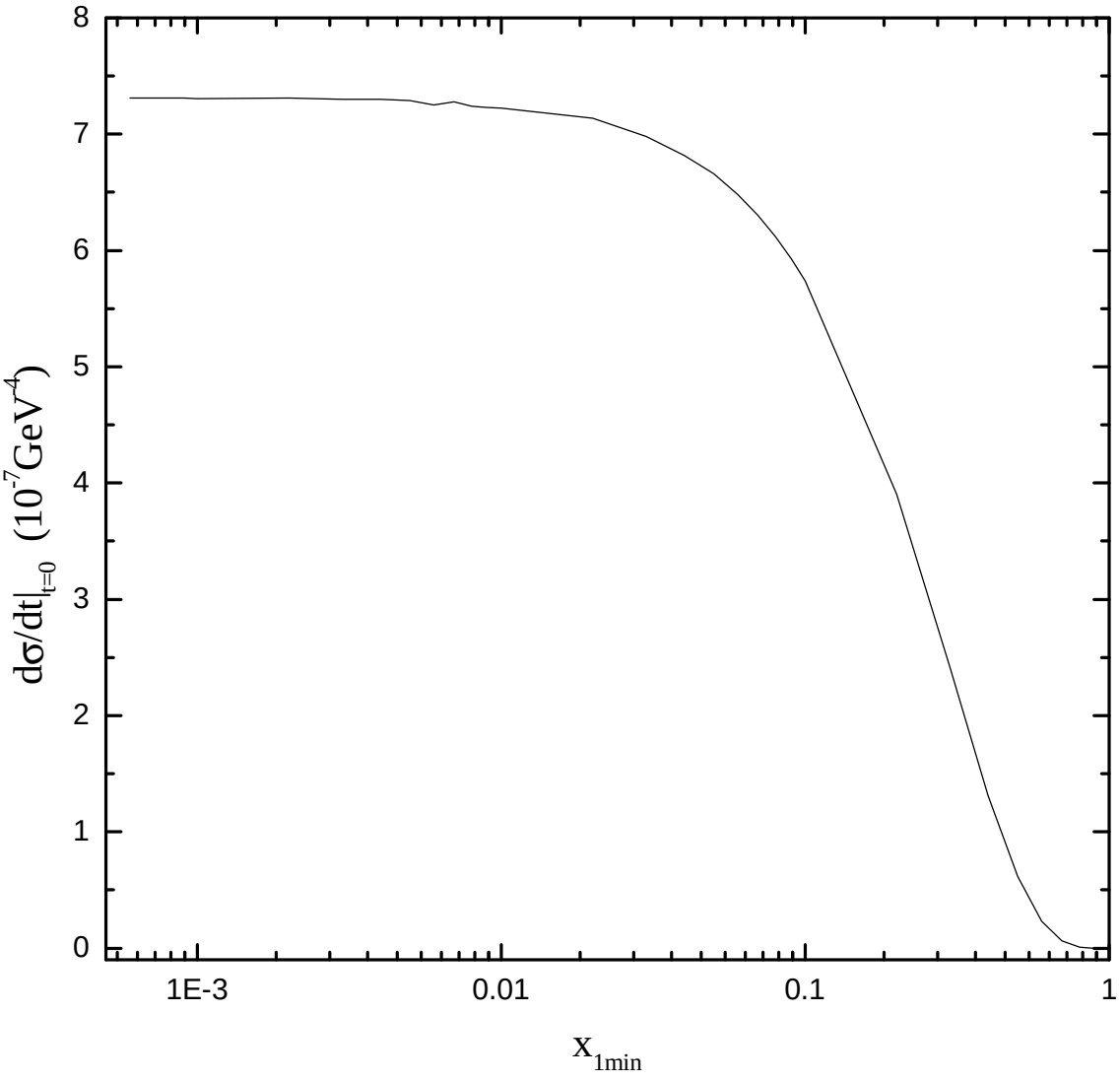

Fig.5(a)

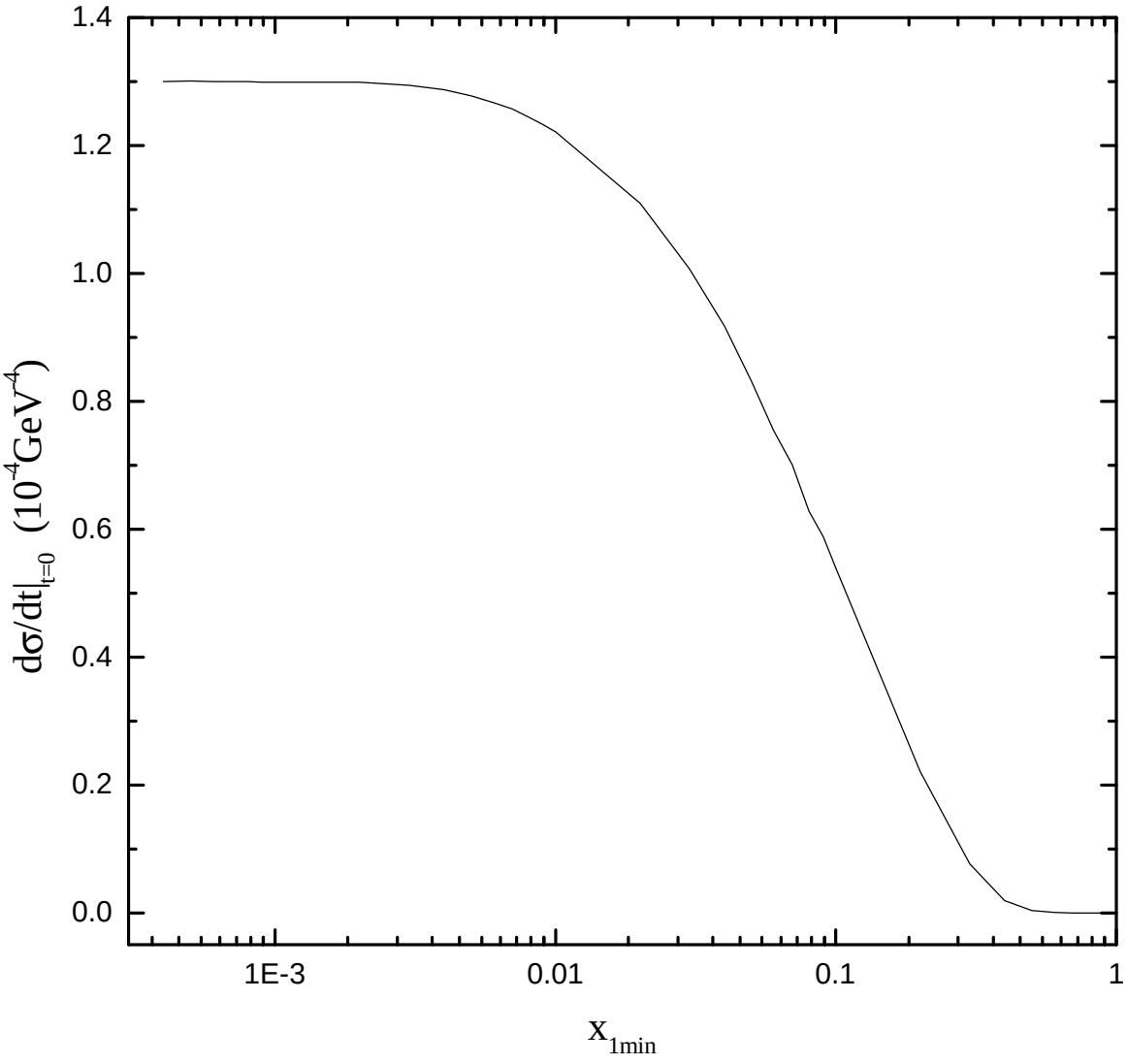

Fig.5(b)